ELSEVIER

International Journal of Mass Spectrometry 218 (2002) 281–297

International Journal of Mass Spectrometry

www.elsevier.com/locate/ijms

# Interaction of $C_3H_3^+$ isomers with molecular nitrogen: IR spectra of $C_3H_3^+$–$(N_2)_n$ clusters ($n = 1$–6)

Otto Dopfer*, Doris Roth, John P. Maier

*Institut für Physikalische Chemie, Universität Basel, Klingelbergstrasse 80, CH-4056 Basel, Switzerland*

Received 19 April 2002; accepted 29 May 2002

**Abstract**

The intermolecular interaction and microsolvation process of isomeric $C_3H_3^+$ ions in molecular nitrogen are characterized by infrared (IR) photodissociation spectroscopy of $C_3H_3^+$–$(N_2)_n$ complexes ($n = 1$–6) and quantum chemical calculations ($n = 0$–4). The rovibrational analysis of the $C_3H_3^+$–$N_2$ spectrum unambiguously reveals the presence of (at least) two $C_3H_3^+$ isomers in the ion source, namely the propargyl ($H_2CCCH^+$) and the cyclopropenyl (c-$C_3H_3^+$) cations. Analysis of the cluster size-dependent vibrational frequency shifts and splittings, the photofragmentation branching ratios, and the results of density functional calculations provides a consistent picture of the microsolvation of c-$C_3H_3^+$ and $H_2CCCH^+$ in inert nitrogen. In the most stable c-$C_3H_3^+$–$(N_2)_n$ complexes, the first three $N_2$ ligands form (nearly) linear and equivalent proton bonds to the three protons of c-$C_3H_3^+$, leading to highly symmetric planar structures with $C_{2v}$ ($n = 1$, 2) and $D_{3h}$ symmetry ($n = 3$). After completion of this first solvation subshell at $n = 3$, further $N_2$ ligands form weaker intermolecular bonds to the C atoms of the nearly planar c-$C_3H_3^+$–$(N_2)_3$ ion core. The dissociation energies of the H-bonds and C-bonds in c-$C_3H_3^+$–$(N_2)_n$ are estimated as $D_0(H) = 900 \pm 130\,cm^{-1}$ and $D_0(C) = 860 \pm 170\,cm^{-1}$, respectively. In the most stable $H_2CCCH^+$–$N_2$ complex, the $N_2$ ligand forms a linear ionic H-bond to the acetylenic C–H group of $H_2CCCH^+$, leading to a planar structure with $C_{2v}$ symmetry. The calculations suggest that the next two ligands bind to the protons of the $CH_2$ group giving rise to planar structures with $C_s$ ($n = 2$) and $C_{2v}$ symmetry ($n = 3$), and these structures are compatible with the observed IR spectra. (Int J Mass Spectrom 218 (2002) 281–297)


*Keywords:* $C_3H_3^+$–$(N_2)_n$ clusters; Ionic complexes; IR spectroscopy; $C_3H_3^+$ isomers; Microsolvation; Intermolecular potential

## 1. Introduction

The $C_3H_3^+$ ion plays a central role for many important phenomena in physical organic chemistry. Two isomers of this fundamental hydrocarbon cation have previously been identified by mass spectrometric [1–5] and spectroscopic techniques [6–11], namely the cyclic cyclopropenyl cation (c-$C_3H_3^+$, Fig. 1a, $D_{3h}$) and the open-chain propargyl cation ($H_2CCCH^+$, Fig. 2a, $C_{2v}$). c-$C_3H_3^+$ is the smallest aromatic cation and found to be ≈25 kcal/mol more stable than $H_2CCCH^+$ [1], in agreement with quantum chemical calculations [11–16]. The latter predict high barriers to interconversion between these two isomers. Other $C_3H_3^+$ isomers, such as $H_3CCC^+$ and $H_2CCHC^+$, are calculated to be significantly less stable than both c-$C_3H_3^+$ and $H_2CCCH^+$ [13–16] and have so far escaped experimental identification.

* Corresponding author. E-mail: otto.dopfer@unibas.ch

1387-3806/02/$ – see front matter 
*PII* S1387-3806(02)00737-6

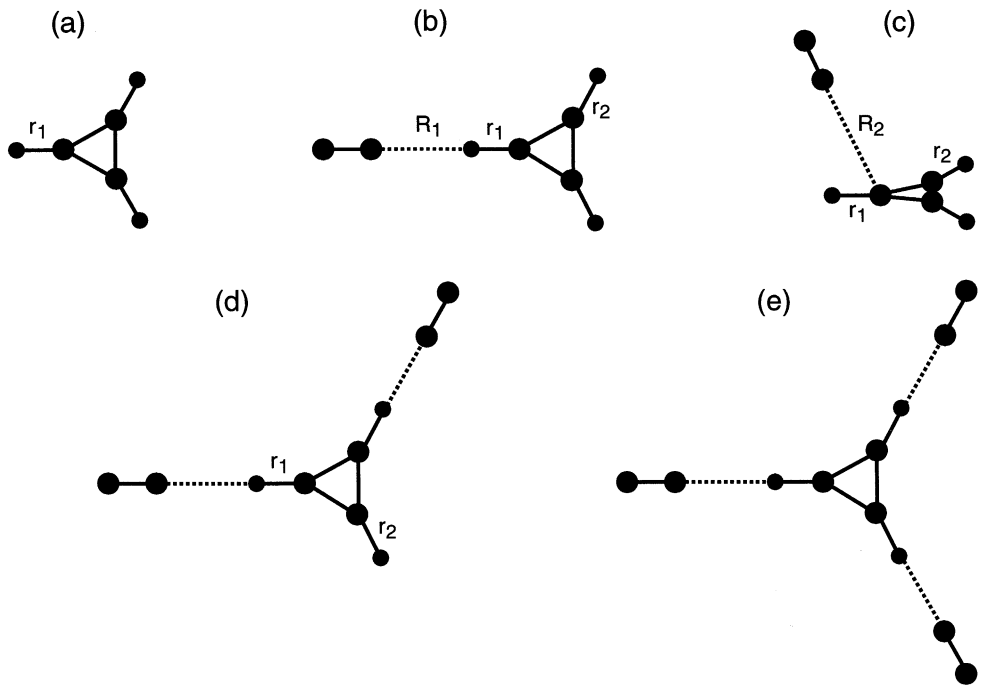


Fig. 1. Structures of c-$C_3H_3^+$–$(N_2)_n$ complexes calculated at the B3LYP/6-31G* level: (a) $n = 0$ ($D_{3h}$); (b) $n = 1$ ($C_{2v}$, global minimum, H-bound structure); (c) $n = 1$ ($C_s$, local minimum, C-bound structure); (d) $n = 2$ ($C_{2v}$); (e) $n = 3$ ($D_{3h}$). See Table 1 for additional structural, energetic, and vibrational data.

Both c-$C_3H_3^+$ and $H_2CCCH^+$ are believed to be central ions in the ion–molecule reaction chemistry of terrestrial and extraterrestrial hydrocarbon plasmas, including interstellar chemistry [17–23], chemistry of planetary atmospheres [24], and soot formation in combustion processes [25–29]. In addition, $C_3H_3^+$ is a common fragment ion observed in the mass spectra of many hydrocarbon molecules [30].

Despite their importance, little spectroscopic information is available for all $C_3H_3^+$ isomers. For example, no gas-phase spectrum of c-$C_3H_3^+$ has been recorded so far. Nonetheless, approximate vibrational frequencies for nearly all fundamentals of this ion have been derived from infrared (IR) and Raman spectra of polycrystalline c-$C_3H_3^+X^-$ salts and their $SO_2$ solutions [6,7] and an IR spectrum of c-$C_3H_3^+$ deposited in a Ne matrix [10]. Gas-phase fundamental frequencies for $\nu_1$–$\nu_7$ of $H_2CCCH^+$ have been measured by photoelectron spectroscopy of the propargyl radical [8,9]. In addition, quantum chemical information of the structure and vibration–rotation parameters are available for both c-$C_3H_3^+$ [11–16,31–33] and $H_2CCCH^+$ [11–16,34–36].

In the present work the intermolecular interaction and microsolvation process of isomeric $C_3H_3^+$ ions in molecular nitrogen are characterized by IR photodissociation spectroscopy of mass-selected $C_3H_3^+$–$(N_2)_n$ complexes ($n$ = 1–6) and quantum chemical calculations ($n$ = 0–4). Previous mass spectrometric studies identified several weakly-bound $C_3H_3^+$–L adducts of $C_3H_3^+$ with stable ligands L and some of them correspond to stabilized intermediates of ion–molecule reactions between $C_3H_3^+$ and L [3–5,37]. The different reactivity of c-$C_3H_3^+$ and $H_2CCCH^+$ toward neutral molecules is often used to distinguish between both isomers in mass spectrometric studies, and $H_2CCCH^+$ is usually more reactive than the more stable c-$C_3H_3^+$ isomer [2–5].

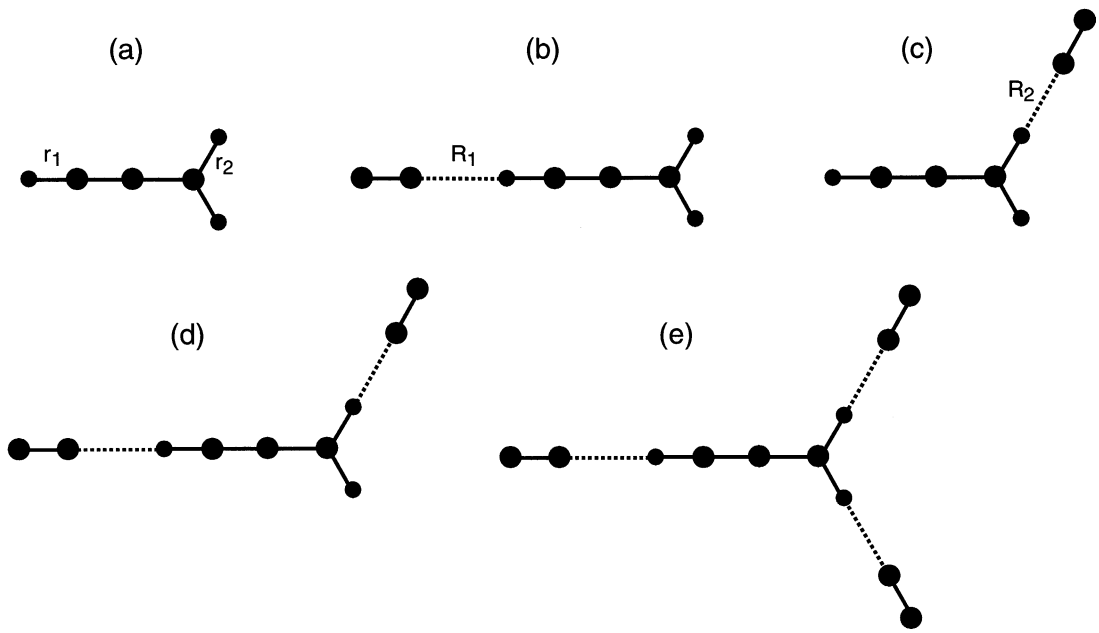


Fig. 2. Structures of $H_2CCCH^+$–$(N_2)_n$ complexes calculated at the B3LYP/6-31G* level: (a) $n = 0$ ($C_{2v}$); (b) $n = 1$ ($C_{2v}$, global minimum); (c) $n = 1$ ($C_s$, local minimum); (d) $n = 2$ ($C_s$); (e) $n = 3$ ($C_{2v}$). See Table 2 for additional structural, energetic, and vibrational data.

The characterization of $C_3H_3^+$–L interaction potentials is desired to improve the understanding of the ion–molecule reaction chemistry of the different $C_3H_3^+$ isomers. Selected ion flow tube studies demonstrated that c-$C_3H_3^+$ and $H_2CCCH^+$ do not react with $N_2$ and no complexes between both constituents have been observed at room temperature [3,4,24]. In the present work weakly-bound $C_3H_3^+$–$(N_2)_n$ complexes are produced in a low temperature supersonic expansion ($T < 50$ K).

In a previous article the IR photodissociation spectrum of the $C_3H_3^+$–$N_2$ dimer in the spectral range of the C–H stretching vibrations has been presented and its interpretation has been guided by ab initio calculations at the MP2(full)/6-311G(2df,2pd) level [11]. The rovibrational analysis of this spectrum revealed for the first time fundamental spectroscopic properties of the two most stable $C_3H_3^+$ isomers and their $N_2$ dimers. The salient results relevant for the present work can be summarized as follows. Electron impact ionization of allene ($H_2CCCH_2$) strongly diluted in a 1:1 mixture of Ar and $N_2$ produces high concentrations of the c-$C_3H_3^+$ and $H_2CCCH^+$ isomers of $C_3H_3^+$ (ratio ≈ 2:1). The observation of the c-$C_3H_3^+$–$N_2$ spectrum is the first spectroscopic identification of the fundamental c-$C_3H_3^+$ ion in the gas phase. According to the calculations, the most stable c-$C_3H_3^+$–$N_2$ dimer has a planar H-bound geometry, with the $N_2$ molecule forming a linear H-bond to one of the three equivalent protons of c-$C_3H_3^+$ (Fig. 1b, $C_{2v}$). This is the only c-$C_3H_3^+$–$N_2$ isomer identified experimentally and the rotational analysis of its IR spectrum provides strong evidence that the c-$C_3H_3^+$ ion is indeed a planar ion with $D_{3h}$ symmetry, in agreement with the calculations. The most stable $H_2CCCH^+$–$N_2$ dimer is predicted to have a planar H-bound structure in which the $N_2$ ligand forms a linear H-bond to the acetylenic proton (Fig. 2b, $C_{2v}$). Again, this is the only $H_2CCCH^+$–$N_2$ isomer identified experimentally, and the rotational analysis of its IR spectrum provides the first spectroscopic evidence that $H_2CCCH^+$ is indeed a planar ion with a linear CCCH backbone ($C_{2v}$), consistent with the ab initio predictions. The structures and relative binding

energies of the various $C_3H_3^+$–$N_2$ dimers can be rationalized by the analysis of the electrostatic and induction forces which dominate the attractive part of the potential in these weakly-bound ion–ligand complexes. The anisotropy of the charge-quadrupole and charge-induced dipole interaction favors for $AH^+$–$N_2$ dimers the linear over the T-shaped orientation, leading to linear –C–H···N–N bonds. The present study of larger $C_3H_3^+$–$(N_2)_n$ complexes ($n$ = 2–6) confirms the interpretation of the $C_3H_3^+$–$N_2$ dimer spectrum and provides further insight into the cluster growth, such as cluster geometries, dissociation energies, and structures of solvation (sub)shells.

## 2. Experimental

IR photodissociation spectra of mass-selected $C_3H_3^+$–$(N_2)_n$ complexes are recorded in a tandem mass spectrometer described previously [38]. The complexes are generated in a pulsed cluster ion source combining a skimmed supersonic expansion with electron impact ionization. The expanded gas mixture contains allene ($H_2CCCH_2$), Ar, and $N_2$ in the ratio 1:100:100 at a stagnation pressure of 5 bar. Electron impact ionization close to the nozzle orifice is followed by ion–molecule reactions to generate various $C_3H_3^+$ isomers. Subsequent three-body association reactions in the high pressure regime of the expansion generate cold $C_3H_3^+$–$(N_2)_n$ complexes. A typical mass spectrum of the ion source under these experimental conditions is discussed in [11]. The analysis of the IR spectrum of $C_3H_3^+$–$N_2$ reveals high abundance of the $H_2CCCH^+$ and c-$C_3H_3^+$ isomers of $C_3H_3^+$ [11]. Efforts to substantially suppress the production of one of these isomers by using various other precursors (such as propyne, 3-chloro-1-propyne, and benzene) failed [11].

The generated cluster ions are extracted through a skimmer into a quadrupole mass spectrometer tuned to the mass of $C_3H_3^+$–$(N_2)_n$. The mass-selected parent ion beam is injected into an octopole ion guide where it is overlapped in space and time with a counter propagating IR laser pulse. Absorption of IR photons in the 3 μm range (2900–3400 $cm^{-1}$) leads to the resonant excitation of vibrational levels lying above the lowest dissociation threshold and subsequent ligand evaporation according to the following photoreaction scheme:

$$C_3H_3^+\text{–}(N_2)_n + \nu_{IR} \rightarrow C_3H_3^+\text{–}(N_2)_n^* \rightarrow C_3H_3^+\text{–}(N_2)_m + (n-m)N_2 \quad (1)$$

Only the rupture of the weak intermolecular bonds is observed under one-photon absorption conditions. The generated $C_3H_3^+$–$(N_2)_m$ photofragment ions are mass selected by a second quadrupole mass spectrometer and monitored as a function of the IR laser frequency ($\nu_{IR}$) to obtain the photodissociation spectra of $C_3H_3^+$–$(N_2)_n$. For larger clusters ($n > 1$) several fragment channels ($m$) are possible and indeed observed. In this case, the IR action spectra are recorded in the two dominant fragment channels. To reduce background signal, mainly arising from metastable decay or collision-induced dissociation of parent ions with residual gas in the octopole region, the cluster ion source is triggered at twice the laser frequency and signals from alternating triggers are subtracted. Pulsed and tunable IR radiation is produced by a single mode optical parametric oscillator (OPO) laser system (bandwidth 0.02 $cm^{-1}$) pumped by a seeded Nd:YAG laser. The OPO laser frequency is calibrated by optoacoustic spectra of HDO recorded simultaneously with the IR action spectra [11,39]. The IR spectra are linearly normalized for laser intensity variations measured with an InSb detector.

## 3. Quantum chemical calculations

Density functional calculations of $C_3H_3^+$–$(N_2)_n$ complexes ($n$ = 0–4) have been carried out at the B3LYP/6-31G* level using GAUSSIAN 98 [40]. The results provide information about the structure and stability of the $C_3H_3^+$ isomers and their $N_2$ complexes. For comparison with the experimental IR spectra, harmonic frequencies and IR intensities are analyzed as well. Comparison with previous ab initio calculations for c-$C_3H_3^+$–$(N_2)_n$ and $H_2CCCH^+$–$(N_2)_n$ with $n = 0$ and $n = 1$ conducted at

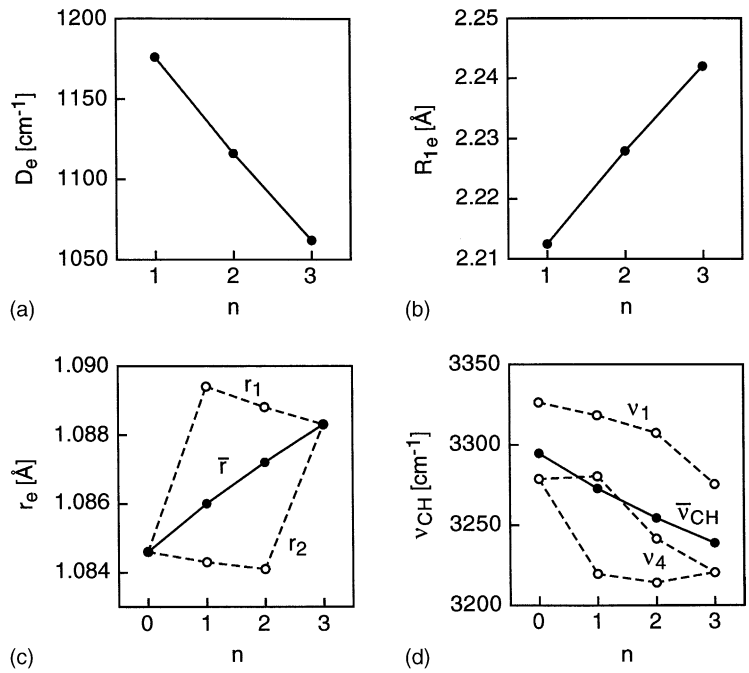


Fig. 3. Selected properties of the intermolecular H-bonds and intramolecular C–H bonds of the most stable c-$C_3H_3^+$–$(N_2)_n$ complexes (Fig. 1) as a function of cluster size calculated at the B3LYP/6-31G* level: (a) binding energy of the H-bond; (b) intermolecular separation of the H-bond; (c) C–H bond lengths; (d) C–H stretching frequencies.

the MP2(full)/6-311G(2df,2pd) level [11] shows that the B3LYP/6-31G* level is sufficient to qualitatively describe the microsolvation of $C_3H_3^+$ isomers in molecular nitrogen. All coordinates are relaxed during the search for stationary points, and the identification of local and global minima is verified by harmonic frequency analysis. Interaction energies are fully counter-poise corrected for basis set superposition error [41]. The results of the calculations are summarized in Figs. 1–4 and Tables 1 and 2. Only the results relevant for the interpretation of the experimental data are presented. Further details are available upon request. As the normal modes of the $C_3H_3^+$ isomers are only weakly affected by $N_2$ complexation, the nomenclature of the $C_3H_3^+$–$(N_2)_n$ cluster modes refers to the $C_3H_3^+$ monomer modes ($\nu_i$), the $N_2$ stretching modes ($\nu_{N–N}$), and the intermolecular bending and stretching modes ($\nu_b$ and $\nu_s$). The analysis of the IR spectrum of $C_3H_3^+$–$N_2$ indicates mainly the presence of the c-$C_3H_3^+$ and $H_2CCCH^+$ isomers in the ion source [11]. Hence, the calculations are restricted to the $N_2$ complexes of these two $C_3H_3^+$ ions.

### 3.1. c-$C_3H_3^+$–$(N_2)_n$

In line with previous calculations, the B3LYP/6-31G* level predicts the c-$C_3H_3^+$ structure to be the lowest-energy isomer of $C_3H_3^+$ (Fig. 1a, $D_{3h}$). Cyclic $C_3H_3^+$ offers several favorable binding sites for quadrupolar $N_2$ ligands. The most stable structure of the c-$C_3H_3^+$–$N_2$ dimer corresponds to the planar H-bound geometry, in which the $N_2$ molecule forms a linear proton bond to one of the three equivalent H atoms of c-$C_3H_3^+$ (Fig. 1b, $C_{2v}$). At the B3LYP/6-31G* level, this intermolecular bond is characterized by a H–N separation of $R_{1e} = 2.2125$ Å, a dissociation energy of $D_e = 1176\,cm^{-1}$, and a harmonic stretching frequency of $\nu_s = 108\,cm^{-1}$. The corresponding values obtained at the higher MP2/6-311G(2df,2pd) level are similar ($R_{1e} = 2.1772\,cm^{-1}$,

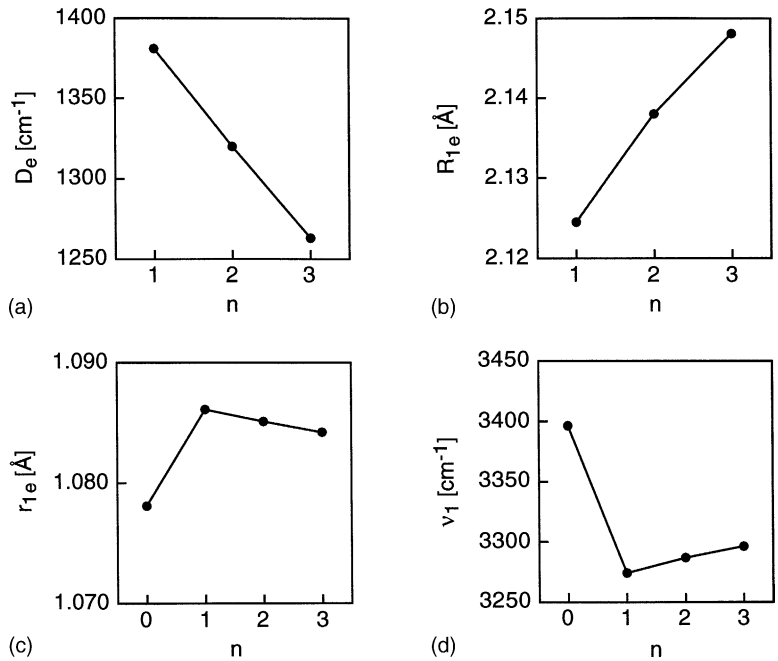


Fig. 4. Selected properties of the intermolecular –C–H$^+\cdots$N–N H-bond and corresponding acetylenic intramolecular C–H bond of the most stable $H_2CCCH^+$–$(N_2)_n$ complexes (Fig. 2) as a function of cluster size calculated at the B3LYP/6-31G* level: (a) binding energy of the H-bond; (b) intermolecular separation of the H-bond; (c) acetylenic C–H bond length; (d) acetylenic C–H stretching frequency ($\nu_1$).

$D_e = 1227\,cm^{-1}$, $\nu_s = 108\,cm^{-1}$ [11]) and justify the application of the B3LYP/6-31G* level to describe the intermolecular c-$C_3H_3^+$–$N_2$ interaction. Similar to the MP2 calculations [11], the C-bound c-$C_3H_3^+$–$N_2$ structure (Fig. 1c, $C_s$) in which the $N_2$ ligand binds to one of the three C atoms of c-$C_3H_3^+$ is found to be a local minimum on the c-$C_3H_3^+$–$N_2$ potential, with $R_{2e} = 2.8641$ Å and $D_e = 793\,cm^{-1}$. The MP2 calculations [11] reveal that the planar side-bound planar structure ($C_{2v}$) is a transition state for the strongly hindered internal c-$C_3H_3^+$ rotation exchanging two equivalent H-bound global minima. Moreover, the π-bound structure in which the $N_2$ ligand binds in a T-shaped fashion to the aromatic π-electron system

Table 1
Dissociation energies, geometrical parameters, harmonic frequencies (unscaled), IR intensities (km/mol) and symmetry species (in parentheses) for the C–H stretching vibrations of c-$C_3H_3^+$–$(N_2)_n$ complexes (Fig. 1) calculated at the B3LYP/6-31G* level

| $n$ | Isomer | $D_e$ ($cm^{-1}$)[a] | $r_{1e}/r_{2e}$ (Å) | $R_{1e}$ (Å) | $R_{2e}$ (Å) | $\nu_4$ ($cm^{-1}$) | $\nu_1$ ($cm^{-1}$) |
|---|---|---|---|---|---|---|---|
| 0 | $D_{3h}$ | | 1.0846 | | | 3278.7 ($e'$/174) | 3326.4 ($a_1'$/0) |
| 1 | $C_{2v}$ | 1176 (H) | 1.0894/1.0843 | 2.2125 | | 3219.6 ($a_1$/342) | 3318.3 ($a_1$/1) |
| | | | | | | 3280.5 ($b_2$/80) | |
| 1 | $C_s$ | 793 (C) | 1.0829/1.0842 | | 2.8641 | 3282.0 ($a''$/81) | 3335.7 ($a'$/2) |
| | | | | | | 3291.3 ($a'$/78) | |
| 2 | $C_{2v}$ | 1116 (H) | 1.0888/1.0841 | 2.2279 | | 3214.3 ($b_2$/456) | 3307.5 ($a_1$/4) |
| | | | | | | 3241.6 ($a_1$/184) | |
| 3 | $D_{3h}$ | 1062 (H) | 1.0883 | 2.2420 | | 3220.6 ($e'$/844) | 3275.6 ($a_1'$/0) |
| 4 | $C_s$ | 605 (C) | 1.0876/1.0864 | ≈2.255 | 2.8981 | 3227.7 ($a''$/397) | 3287.7 ($a'$/6) |
| | | 1021 (H) | | | | 3236.9 ($a'$/380) | |

[a] H and C indicate the binding energies of H-bound and C-bound $N_2$ ligands, respectively.

Table 2
Dissociation energies, geometrical parameters, harmonic frequencies (unscaled), IR intensities (km/mol) and symmetry species (in parentheses) for the C–H stretching vibrations of $H_2CCCH^+$–$(N_2)_n$ complexes (Fig. 2) calculated at the B3LYP/6-31G* level

| $n$ | Isomer | $D_e$ ($cm^{-1}$)[a] | $r_{1e}$ (Å) | $r_{2e}$ (Å) | $R_{1e}$ (Å) | $R_{2e}$ (Å) | $\nu_2$ ($cm^{-1}$) | $\nu_9$ ($cm^{-1}$) | $\nu_1$ ($cm^{-1}$) |
|---|---|---|---|---|---|---|---|---|---|
| 0 | $C_{2v}$ | | 1.0781 | 1.0927 | | | 3135.1 ($a_1$/28) | 3233.9 ($b_2$/41) | 3396.4 ($a_1$/115) |
| 1 | $C_{2v}$ | 1381 (CH) | 1.0861 | 1.0921 | 2.1245 | | 3139.4 ($a_1$/26) | 3237.7 ($b_2$/36) | 3274.2 ($a_1$/536) |
| 1 | $C_s$ | 1098 ($CH_2$) | 1.0776 | 1.0925/1.0959 | | 2.2603 | 3105.7 ($a'$/165) | 3216.5 ($a'$/105) | 3400.6 ($a'$/117) |
| 2 | $C_s$ | 1320 (CH)<br>1038 ($CH_2$) | 1.0851 | 1.0922/1.0953 | 2.1380 | 2.2730 | 3111.9 ($a'$/161) | 3219.7 ($a'$/99) | 3286.9 ($a'$/519) |
| 3 | $C_{2v}$ | 1263 (CH)<br>971 ($CH_2$) | 1.0842 | 1.0950 | 2.1481 | 2.2933 | 3098.8 ($a_1$/179) | 3198.0 ($b_2$/231) | 3296.5 ($a_1$/507) |

[a] CH and $CH_2$ indicate the binding energies of $N_2$ ligands attached to a proton of the CH and $CH_2$ groups of $H_2CCCH^+$, respectively.

of c-$C_3H_3^+$ ($C_{3v}$) is identified as a transition state between the C-bound local minima [11].

As the $C_3H_3^+$–$N_2$ interaction is much stronger than the $N_2$–$N_2$ interaction [42] for any orientation, the initial microsolvation process of $C_3H_3^+$ in molecular nitrogen is predominantly determined by the $C_3H_3^+$–$N_2$ interaction. According to the c-$C_3H_3^+$–$N_2$ dimer potential, the cluster growth in c-$C_3H_3^+$–$(N_2)_n$ is expected to begin with $N_2$ complexation of the three equivalent protons. Indeed, the most stable structures of c-$C_3H_3^+$–$(N_2)_n$ with $n$ = 1–3 are planar and highly symmetric (Fig. 1). They feature equivalent and (nearly) linear intermolecular proton bonds with $C_{2v}$ ($n$ = 1, Fig. 1b), $C_{2v}$ ($n$ = 2, Fig. 1d), and $D_{3h}$ symmetry ($n$ = 3, Fig. 1e), respectively. Significant noncooperative three-body effects cause the intermolecular bonds to become weaker and longer as the number of equivalent proton bonds in c-$C_3H_3^+$–$(N_2)_n$ increases: $D_e$ decreases almost linearly from 1176 $cm^{-1}$ ($n$ = 1) to 1062 $cm^{-1}$ ($n$ = 3) by ≈60 $cm^{-1}$ per $N_2$ molecule (Fig. 3a), and at the same time $R_{1e}$ increases by ≈0.015 Å per $N_2$ ligand (Fig. 3b). As expected, the largest structural perturbation of c-$C_3H_3^+$ upon $N_2$ complexation is a significant lengthening of the C–H bonds involved in H-bonding ($r_1$), and simultaneously a small contraction of the free C–H bonds ($r_2$). The net effect is an almost linear increase of the averaged C–H bond length by 0.0012 Å per $N_2$ ligand (Fig. 3c). These structural changes are also mirrored in the three C–H stretching frequencies, $\nu_4(e')$ and $\nu_1(a_1')$. The averaged value for the C–H stretch frequencies decreases by ≈19 $cm^{-1}$ per $N_2$ ligand (Fig. 3d). Symmetry reduction from $D_{3h}$ ($n$ = 0, 3) to $C_{2v}$ ($n$ = 1, 2) causes the doubly degenerate C–H stretching mode, $\nu_4(e')$, to split into two components with $a_1$ and $b_2$ symmetry, respectively (Table 1, Fig. 3d). The splitting is calculated as 60.9 and 27.3 $cm^{-1}$ for $n$ = 1 and 2, respectively. The $\nu_4(a_1)$ mode of the dimer is predominantly the bound C–H stretch mode and features thus a large red shift upon H-bonding, $\Delta\nu_4(a_1) = -59.1\,cm^{-1}$. In contrast, the $\nu_4(b_2)$ mode is mainly the antisymmetric stretch of the two free C–H bonds and experiences only a small blue shift, $\Delta\nu_4(b_2) = 1.8\,cm^{-1}$. In the trimer (Fig. 1d), the $\nu_4(a_1)$ and $\nu_4(b_2)$ modes correspond mainly to the symmetric and antisymmetric stretch vibrations of the two bound C–H bonds and are thus both largely red shifted with respect to the monomer value: $\Delta\nu_4(a_1) = -64.4\,cm^{-1}$ and $\Delta\nu_4(b_2) = -37.1\,cm^{-1}$, respectively (Fig. 3d).

After the first solvation subshell is filled with the formation of three equivalent H-bonds in c-$C_3H_3^+$–$(N_2)_3$, further $N_2$ ligands are expected to form intermolecular C-bonds, because this binding site corresponds to a local minimum on the dimer potential. Indeed, calculations for c-$C_3H_3^+$–$(N_2)_4$ reveal a minimum structure with $C_s$ symmetry in which one C-bound $N_2$ ligand is attached to a nearly planar c-$C_3H_3^+$–$(N_2)_3$ ion core (Table 1). In contrast to H-bonding, C-bound $N_2$ ligands strengthen and shorten all C–H bonds, leading to an increase in all three C–H stretching frequencies (Table 1). Consequently, solvating the c-$C_3H_3^+$–$(N_2)_3$ ion core with C-bound $N_2$ ligands is expected to cause a rise in

both the $\nu_4$ and $\nu_1$ frequencies of c-$C_3H_3^+$–$(N_2)_n$ for $n \geq 4$. Moreover, the $\nu_4$ splitting in C-bound c-$C_3H_3^+$–$N_2$ and c-$C_3H_3^+$–$(N_2)_4$ due to symmetry reduction from $D_{3h}$ to $C_s$ is rather small ($\approx$10 cm$^{-1}$) compared to the splitting caused by H-bonding in the c-$C_3H_3^+$–$N_2$ and c-$C_3H_3^+$–$(N_2)_2$ complexes (Table 1). Due to noncooperative effects, the C-bond and the three H-bonds in c-$C_3H_3^+$–$(N_2)_4$ are weaker than the corresponding bonds in the C-bound dimer and H-bound tetramer: $D_e$ = 605 vs. 793 cm$^{-1}$ and $D_e$ = 1021 vs. 1062 cm$^{-1}$, respectively (Table 1).

### 3.2. $H_2CCCH^+$–$(N_2)_n$

The planar $H_2CCCH^+$ ion (Fig. 2a, $C_{2v}$) is calculated to be 25.3 kcal/mol less stable than c-$C_3H_3^+$ (including harmonic zero-point corrections), in good agreement with the experimental measurement ($\approx$25 kcal/mol [1]). The global minimum on the intermolecular $H_2CCCH^+$–$N_2$ dimer potential corresponds to a planar H-bound structure in which the $N_2$ ligand forms a linear H-bond to the acetylenic proton (Fig. 2b, $C_{2v}$). The intermolecular H-bond is characterized by $R_{1e}$ = 2.1245 Å, $D_e$ = 1381 cm$^{-1}$, and $\nu_s$ = 120 cm$^{-1}$ (Table 2). The corresponding data at the MP2/6-311G(2df,2pd) level are $R_e$ = 2.0916 Å, $D_e$ = 1373 cm$^{-1}$, and $\nu_s$ = 120 cm$^{-1}$ [11]. H-bonding leads to a large elongation of the acetylenic C–H bond ($\Delta r_1$ = 0.008 Å), accompanied by a large red shift ($\Delta\nu_1 = -122.2$ cm$^{-1}$) and IR enhancement (factor 4.7) of the corresponding C–H stretching fundamental ($\nu_1$). The C–H bonds of the $CH_2$ group slightly contract upon complexation of the acetylenic C–H bond, leading to a small increase of the corresponding symmetric and antisymmetric C–H stretch frequencies, $\Delta\nu_2$ = 4.3 cm$^{-1}$ and $\Delta\nu_9$ = 3.8 cm$^{-1}$, respectively. The planar H-bound $N_2$–$H_2CCCH^+$ dimer in which the $N_2$ molecule forms a nearly linear H-bond to one proton of the $CH_2$ group corresponds to a local minimum with $D_e$ = 1098 cm$^{-1}$ and $R_{2e}$ = 2.2603 Å (Fig. 2c, $C_s$). Both local C–H stretch modes of the $CH_2$ group are strongly coupled in free $H_2CCCH^+$, producing a large splitting of 98.8 cm$^{-1}$ between $\nu_2$ and $\nu_9$. As weak H-bonding to one of the $CH_2$ protons does not completely decouple both modes, they are both shifted to lower frequency upon complexation, $\Delta\nu_2 = -29.4$ cm$^{-1}$ and $\Delta\nu_9 = -17.4$ cm$^{-1}$. The effects of H-bonding are larger for $\nu_2$ because this mode has more bound C–H stretch character compared to $\nu_9$. Interestingly, complexation at the $CH_2$ group slightly strengthens the acetylenic C–H bond ($\Delta r_{1e} = -0.0005$ Å) leading to a small blue shift of $\Delta\nu_1$ = 4.2 cm$^{-1}$.

According to the two H-bound minima on the dimer potential, $H_2CCCH^+$–$N_2$ and $N_2$–$H_2CCCH^+$, the microsolvation of $H_2CCCH^+$ in $N_2$ is expected to begin with solvation of the acetylenic C–H proton and subsequently the two protons of the $CH_2$ group, leading to planar equilibrium structures with $C_{2v}$ ($n$ = 1, Fig. 2b), $C_s$ ($n$ = 2, Fig. 2d), and $C_{2v}$ symmetry ($n$ = 3, Fig. 2e). Similar to the c-$C_3H_3^+$–$(N_2)_n$ clusters, noncooperative three-body forces cause the intermolecular proton bonds to become weaker as the number of ligands in the cluster increases (Fig. 4). For example, complexation at the $CH_2$ group causes the H-bond to the acetylenic C–H group to become longer and more fragile: $R_{1e}$ = 2.1245, 2.1380, and 2.1481 Å and $D_e$ = 1381, 1320, and 1263 cm$^{-1}$ for $n$ = 1–3, respectively (Fig. 4a and b). These changes in H-bonding are also reflected in the C–H bond lengths and stretching frequencies. For example, complexation at the $CH_2$ group causes the acetylenic C–H bond to become shorter and stronger: $r_{1e}$ = 1.0861, 1.0851, and 1.0842 Å and $\nu_1$ = 3274, 3287, and 3297 cm$^{-1}$ for $n$ = 1–3, respectively (Fig. 4c and d).

## 4. Experimental results and discussion

Fig. 5 reproduces the IR spectra of $C_3H_3^+$–$(N_2)_n$ for $n$ = 1–6 in the spectral range between 2970 and 3340 cm$^{-1}$. They are recorded in the dominant $C_3H_3^+$–$(N_2)_m$ fragment channel (indicated as $n \rightarrow m$). The observed transitions are labeled A–H, and their positions, widths, and suggested assignments are summarized in Table 3. The interpretation of the transitions are based on the analysis of their positions and band profiles as well as the comparison with the

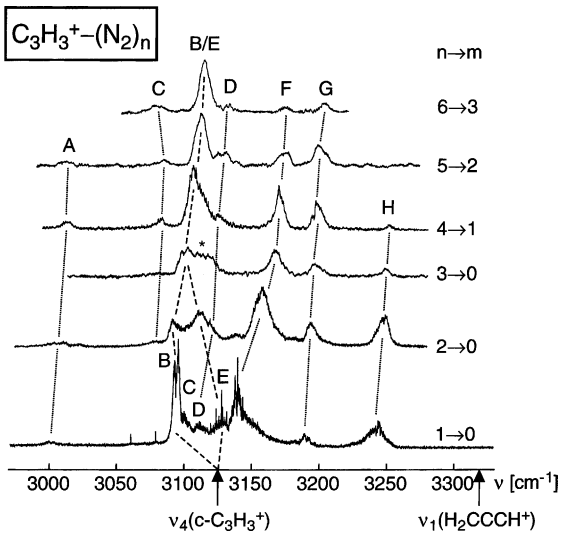


Fig. 5. IR photodissociation spectra of $C_3H_3^+$–$(N_2)_n$ ($n$ = 1–6) recorded in the $C_3H_3^+$–$(N_2)_m$ fragment channel (indicated as $n \rightarrow m$) between 2970 and 3340 $cm^{-1}$. The observed transitions are labeled A–H and their suggested assignments are listed in Table 3. The transitions B and E connected by dashed lines are assigned to the $\nu_4$ band(s) of c-$C_3H_3^+$–$(N_2)_n$. All other transitions (A, C, D, F, G, H; connected by dotted lines) are attributed to $H_2CCCH^+$–$(N_2)_n$. The arrows below the wavelength scale indicate the positions of $\nu_4$ of free c-$C_3H_3^+$ ($3125 \pm 4\,cm^{-1}$ [11]) and $\nu_1$ of free $H_2CCCH^+$ ($3319 \pm 10\,cm^{-1}$ [9]).

quantum chemical calculations. A thorough analysis of the dimer spectrum ($n$ = 1) is presented in [11] and only the salient results are repeated here.

### 4.1. The $\nu_4$ vibration of c-$C_3H_3^+$–$(N_2)_n$

According to previous spectra of c-$C_3H_3^+$ in salt crystals, $SO_2$ solutions, and Ne matrices as well as quantum chemical calculations, only the strongly IR active $\nu_4$ mode is expected to be observed with significant intensity in the IR spectra of c-$C_3H_3^+$–$(N_2)_n$ in the spectral range investigated. Symmetry reduction from $D_{3h}$ ($n$ = 0) to $C_{2v}$ ($n$ = 1) causes the $\nu_4(e')$ fundamental of c-$C_3H_3^+$ to split into two components in H-bound c-$C_3H_3^+$–$N_2$ (Table 1): a perpendicular component with a small blue shift, $\nu_4(b_2)$, and a parallel component with a larger red shift, $\nu_4(a_1)$. The bands B ($3094\,cm^{-1}$) and E ($3129\,cm^{-1}$) in the spectrum of the $C_3H_3^+$–$N_2$ dimer have unambiguously been assigned to the $\nu_4(a_1)$ and $\nu_4(b_2)$ fundamentals of the H-bound c-$C_3H_3^+$–$N_2$ structure shown in Fig. 1b [11]. The assignments are based on the frequencies, IR intensities, rotational analysis, the nuclear spin statistical weights arising from two equivalent protons, and the comparison with ab initio calculations. In addition, the frequency of free c-$C_3H_3^+$ could accurately be derived as $\nu_4(e') = 3125 \pm 4\,cm^{-1}$ (indicated by the arrow in Fig. 5), in good agreement with previous IR spectra of c-$C_3H_3^+$ recorded in a Ne matrix ($3130.4 \pm 1\,cm^{-1}$ [10]) and in $SO_2$ solutions ($3138\,cm^{-1}$ [7]). The rovibrational analysis shows that the H-bound global minimum of c-$C_3H_3^+$–$N_2$ is the only c-$C_3H_3^+$–$N_2$ isomer unambiguously detected in the $C_3H_3^+$–$N_2$ spectrum

Table 3
Positions ($cm^{-1}$), widths (FWHM, in parentheses), and suggested assignments of the observed transitions in the IR photodissociation spectra of $C_3H_3^+$–$(N_2)_n$ ($n$ = 1–6) in Figs. 5 and 9

| $n \rightarrow m$ | A | B | C | D | E | F | G | H |
|---|---|---|---|---|---|---|---|---|
| $1 \rightarrow 0$[a] | 3001 (6) | 3094 (5) | 3104.91[b] | 3113 (10) | 3128.75[b] | 3139 (4) | 3191 (6) | 3243 (13) |
| $2 \rightarrow 0$ | 3011 (24) | 3091 (7) | 3078 (8) | 3118 (4) | 3111 (10) | 3157 (14) | 3194 (8) | 3248 (9) |
| $3 \rightarrow 0$ | | 3101 (12)[c] | | | 3101 (12) | 3167 (9) | 3197 (8) | 3249 (6) |
| $3 \rightarrow 1$ | 3020 (3) | | 3083 (5) | 3118 (4) | | 3165 (5) | 3194 (7) | 3250 (4) |
| $4 \rightarrow 1$ | 3013 (7) | 3106 (12) | 3082 (7) | 3124 (8) | 3106 (12) | 3170 (6) | 3197 (10) | 3251 (7) |
| $5 \rightarrow 2$ | 3011 (12) | 3112 (11) | 3084 (7) | 3127 (10) | 3112 (11) | 3173 (10) | 3199 (11) | |
| $6 \rightarrow 3$ | | 3114 (9) | 3079 (13) | 3132 (6) | 3114 (9) | 3174 (8) | 3203 (6) | |
| Isomer | $H_2CCCH^+$ | c-$C_3H_3^+$ | $H_2CCCH^+$ | $H_2CCCH^+$ | c-$C_3H_3^+$ | $H_2CCCH^+$ | $H_2CCCH^+$ | $H_2CCCH^+$ |
| Assignment | $2\nu_4$ | $\nu_4$ | $\nu_3 + \nu_{7/10}$ | $\nu_2$?, $\nu_3 + \nu_{10/7}$? | $\nu_4$ | $\nu_1$ | $\nu_3 + \nu_5$? | $\nu_3 + \nu_5$? |

[a] Ref. [11].
[b] For the perpendicular transitions C and E in the dimer spectrum the fitted band origins, $\nu_0$, are listed.
[c] This peak has as side shoulder centered at 3115 (16) $cm^{-1}$.

in Fig. 5 [11]. This observation is in agreement with the ab initio and density functional calculations, which predict that the side-bound and π-bound structures of c-$C_3H_3^+$–$N_2$ are not minima on the intermolecular potential but transition states. The population of the C-bound local minima (Fig. 1c) appears to be below the detection limit, probably because of a low isomerization barrier toward the H-bound global minima [11] and/or spectral congestion in this spectral range.

The calculations suggest that the most stable c-$C_3H_3^+$–$(N_2)_2$ trimer has a planar structure with two equivalent H-bound $N_2$ ligands (Fig. 1d, $C_{2v}$). Similar to the H-bound dimer, the $\nu_4$ mode of this trimer is split into two components with $a_1$ and $b_2$ symmetry and they are observed at $\nu_4(a_1) = 3111\,cm^{-1}$ (band E) and $\nu_4(b_2) = 3091\,cm^{-1}$ (band B), respectively. The measured splitting of $20\,cm^{-1}$ is somewhat smaller than the calculated one ($27\,cm^{-1}$). Moreover, the higher frequency $a_1$ component is predicted to be ≈2.5 times more intense than the lower frequency $b_2$ component, in good agreement with the experimental spectrum. The calculated global minimum of the c-$C_3H_3^+$–$(N_2)_3$ tetramer has a planar structure with three equivalent H-bound $N_2$ ligands (Fig. 1e, $D_{3h}$). The $\nu_4$ mode is not split for this structure and assigned to the intense transition at $3101\,cm^{-1}$. The first $N_2$ solvation subshell is closed at $n = 3$ and further $N_2$ ligands are expected to form C-bonds to the planar c-$C_3H_3^+$–$(N_2)_3$ core, because the C-bond is a local minimum on the dimer potential. The calculations show that the formation of intermolecular C-bonds strengthens the intramolecular C–H bonds leading to an increase in the C–H stretching frequencies. In addition, the C-bonds remove the threefold symmetry and should split the $\nu_4$ fundamental into its two components with similar IR intensity. However, the splitting is predicted to be of the order of the typical widths of the bands (≈$10\,cm^{-1}$) and may not be completely resolved. For example, in the C-bound dimer and the c-$C_3H_3^+$–$(N_2)_4$ pentamer it is calculated to be smaller than $10\,cm^{-1}$ (Table 1). Thus, complexation of the c-$C_3H_3^+$–$(N_2)_3$ core ion with equivalent C-bound $N_2$ ligands should produce single and possibly slightly broadened $\nu_4$ bands with

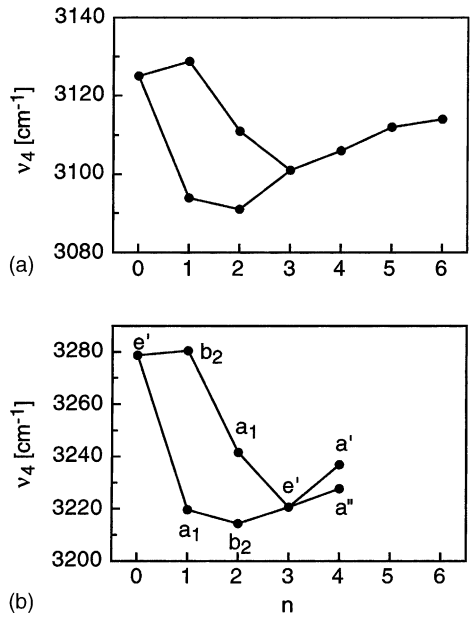


Fig. 6. Comparison between experimental (a) and calculated (b) $\nu_4$ frequencies of the most stable c-$C_3H_3^+$–$(N_2)_n$ clusters. For the calculated fundamentals the symmetry species are listed as well.

increasing frequency as $n$ increases. Indeed, the IR spectra of c-$C_3H_3^+$–$(N_2)_n$ with $n = 4$–6 show single intense bands at 3106, 3112, and $3114\,cm^{-1}$ which can readily be assigned to the $\nu_4$ fundamental(s) of these cluster ions. The incremental $\nu_4$ blue shift of the $n = 4$ complex with respect to the $n = 3$ complex, $\Delta\nu_4 = 5\,cm^{-1}$, is compatible with the calculated averaged shift of both $\nu_4$ components, $\Delta\nu_4 = 12\,cm^{-1}$.

Fig. 6 compares the observed $\nu_4$ frequencies of the most stable c-$C_3H_3^+$–$(N_2)_n$ complexes (a) with those predicted at the B3LYP/6-31G* level (b). The overall good agreement of both pattern strongly supports the given assignments. Moreover, the size-dependent $\nu_4$ frequencies reflect directly the substructure of the first $N_2$ solvation shell around the c-$C_3H_3^+$ ion. $N_2$ ligands in the first subshell ($n = 1$–3) form equivalent and (nearly) linear H-bonds which destabilize the C–H bonds of c-$C_3H_3^+$ leading to a decrease of the averaged $\nu_4$ frequency as $n$ increases. On the other hand, $N_2$ ligands in the second subshell form equivalent C-bonds which stabilize the C–H bonds of c-$C_3H_3^+$

leading to an increase of the averaged $\nu_4$ frequency. Presumably up to six ligands can form C-bonds (three above and three below the c-$C_3H_3^+$ plane), implying that the second subshell corresponds to the size range $n = 4$–9. It is not clear how many $N_2$ ligands are required to complete the first solvation shell around the central c-$C_3H_3^+$ ion. Moreover, although the incremental $\nu_4$ frequency shift decreases monotonically for $n = 4$–6 (Fig. 6a), it is apparently not fully converged at $n = 6$. However, convergence at this cluster size is not expected because the first solvation shell is not completed yet. Interestingly, the $\nu_4$ frequency of the $n = 6$ cluster is very close to the frequency of the bare ion, and the total shift ($\Delta\nu_4 = -11\,cm^{-1}$) is smaller than those of the smaller cluster sizes. This observation emphasizes the large effects of asymmetric solvation of the central ion within an incomplete first solvation shell.

So far, the $\nu_4$ transitions have all been assigned to the most stable c-$C_3H_3^+$–$(N_2)_n$ clusters (see the bands B and E connected by dashed lines in Fig. 5). The only indication for the existence of a less stable isomer is observed in the spectrum of the $n = 3$ complex, where a second band at 3115 $cm^{-1}$ (indicated by an asterisk in Fig. 5) is observed in the range of $\nu_4$, in addition to the $\nu_4$ fundamental assigned to the $D_{3h}$ symmetric global minimum structure (3101 $cm^{-1}$). The 3115 $cm^{-1}$ band is shifted to the blue of the $n = 2$ absorptions and may thus be attributed to a less stable $n = 3$ isomer featuring two H-bonds and one C-bond, because C-bonding stabilizes the C–H bonds. The analysis of the photofragmentation branching ratios in Section 4.4 strongly indicates that the $\nu_4$ fundamental is the only transition of c-$C_3H_3^+$–$(N_2)_n$ occurring in the spectral range investigated. Hence, all other transitions observed in the spectra of $C_3H_3^+$–$(N_2)_n$ have to be attributed to clusters with another $C_3H_3^+$ isomer.

### 4.2. The $\nu_1$ vibration of $H_2CCCH^+$–$(N_2)_n$

The rovibrational analysis of band C in the spectrum of $C_3H_3^+$–$N_2$ unambiguously proves the presence of $H_2CCCH^+$ (Fig. 2a) and its H-bound $H_2CCCH^+$–$N_2$ dimer (Fig. 2b) in the expansion [11]. According to the ab initio [11] and density functional calculations (Table 2), $\nu_1$ is by far the strongest IR active fundamental of this dimer in the investigated spectral range. It corresponds to the stretching mode of the acetylenic C–H bond adjacent to the intermolecular proton bond. The corresponding gas-phase frequency of bare $H_2CCCH^+$ has been measured as $\nu_1 = 3319\,cm^{-1}$ (indicated by an arrow in Fig. 5) [9] and no intense absorption is observed in the IR spectrum of $C_3H_3^+$–$N_2$ within 80 $cm^{-1}$ of this value. Consequently, the $\nu_1$ fundamental of any $H_2CCCH^+$–$N_2$ isomer present in the expansion has to feature a substantial $\nu_1$ shift which can only occur when the $N_2$ ligand binds to the terminal acetylenic C–H group of $H_2CCCH^+$. Apparently, the H-bound $H_2CCCH^+$–$N_2$ minimum in Fig. 2b is the only $H_2CCCH^+$–$N_2$ isomer with significant abundance in the expansion. This structure is also predicted to be the global minimum of this dimer. H-bonding induces a large red shift and IR intensity enhancement of $\nu_1$ (Table 2) owing to a significant destabilization of the acetylenic C–H bond. Consequently, the intense band F at 3139 $cm^{-1}$ in the spectrum of $C_3H_3^+$–$N_2$ has been assigned to $\nu_1$ of H-bound $H_2CCCH^+$–$N_2$ [11]. The measured red shift upon complexation ($-180\,cm^{-1}$) is somewhat larger than the calculated one ($-122\,cm^{-1}$).

As can be seen from Fig. 5, band F assigned to $\nu_1$ of H-bound $H_2CCCH^+$–$N_2$ displays significant monotonic blue shifts upon complexation with additional $N_2$ ligands (Fig. 7a). Apparently, the acetylenic C–H bond is stabilized by the addition of further $N_2$ ligands, consistent with a reduction in the strength of the adjacent intermolecular proton bond to the first $N_2$ ligand (Fig. 4a). This behavior is typical for solvation of a H-bound $AH^+$–L dimer with further ligands L [43–45] and has previously been observed for several $N_2$ containing ion–ligand complexes, such as $SiOH^+$–$(N_2)_n$ and $C_6H_5OH^+$–$(N_2)_n$ [45,46]. It strongly supports the assignment of band F to $\nu_1$ of H-bound $H_2CCCH^+$–$N_2$. The measured incremental blue shifts upon further complexation of H-bound $H_2CCCH^+$–$N_2$ decrease in a monotonic fashion as a function of $n$: $\Delta\nu_1 = 18$, 10, 3, 3, and 1 $cm^{-1}$ for $n = 2$–6, respectively (Fig. 7a). The shifts of the

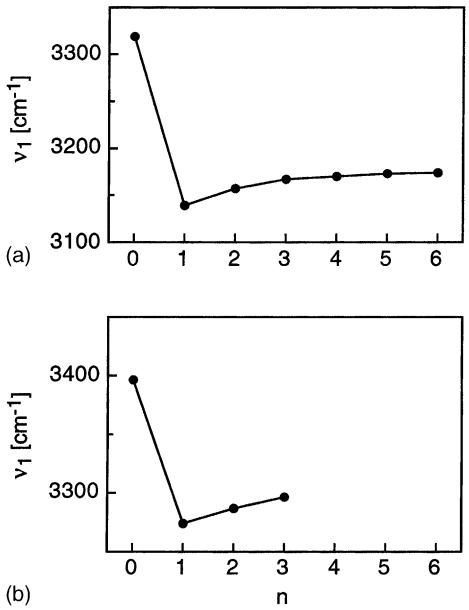


Fig. 7. Comparison between experimental (a) and calculated (b) $\nu_1$ frequencies of the most stable $H_2CCCH^+$–$(N_2)_n$ clusters.

second and third $N_2$ ligand are much larger than those of subsequent ligands, indicating that both groups of ligands have qualitatively different binding sites. This observation is taken as evidence that the second and third ligand are forming H-bonds to the two protons of the $CH_2$ group (Fig. 2d and e). Indeed, these planar structures are calculated to be stable minima and $N_2$ complexation at the $CH_2$ group is stabilizing the acetylenic C–H bond. The blue shifts of $\nu_1$ of 13 and 10 $cm^{-1}$ calculated for these $n = 2$, 3 structures are compatible with the observed shifts of 18 and 10 $cm^{-1}$, respectively (Fig. 7b). Apparently, further $N_2$ ligands ($n > 3$) occupy less favorable binding sites which have a smaller influence on the acetylenic C–H stretch.

Finally, it is noted that the characteristic $\nu_1$ band shifts of $H_2CCCH^+$–$(N_2)_n$ would also be compatible with a cluster growth scenario different from that described in Fig. 2. In this alternative model, the H-bound $H_2CCCH^+$–$N_2$ dimer in Fig. 2b is further solvated by $N_2$ ligands filling an equatorial solvation ring around the acetylenic proton. Similar cluster structures have been inferred for $HCO^+$–$Ar_n$ and $HN_2^+$–$Ar_n$ from their $\nu_1$ spectral shifts [38,44] which are qualitatively similar to those observed for $H_2CCCH^+$–$(N_2)_n$. However, efforts to locate the corresponding minimum on the $H_2CCCH^+$–$(N_2)_2$ potential by gradient optimization failed. Thus, although such cluster geometries can not be ruled out completely, the cluster growth described in Fig. 2 is presently favored.

### 4.3. Other vibrations

In contrast to the $\nu_1$ vibration of $H_2CCCH^+$–$(N_2)_n$ and the $\nu_4$ vibration(s) of c-$C_3H_3^+$–$(N_2)_n$, the assignments of the other bands (i.e., A, C, D, G, H) are less certain. The analysis of the photofragmentation branching ratios presented in Section 4.4 suggests that the latter bands are almost certainly not arising from isomeric c-$C_3H_3^+$–$(N_2)_n$ clusters. Consequently, they are most likely due to $H_2CCCH^+$–$(N_2)_n$ and this scenario has been followed in [11] to obtain the tentative assignments listed in Table 3. The reader is referred to [11] for a more detailed discussion of these suggested assignments and only the salient results are summarized here.

The rotational structure of band C in the dimer spectrum with origin at 3104.91 $cm^{-1}$ is only compatible with the H-bound $CH_2CCCH^+$–$N_2$ structure shown in Fig. 2b and this vibration has been attributed to either $\nu_3 + \nu_7$ or $\nu_3 + \nu_{10}$ [11]. The $\nu_3$ mode is the acetylenic C–C stretch with a frequency of 2100 $cm^{-1}$ and has by far the largest IR intensity of all vibrations of bare $H_2CCCH^+$ [10,11,35]. Hence, combination tones involving $\nu_3$ are expected in the IR spectra of $H_2CCCH^+$–$(N_2)_n$. The $\nu_7$ and $\nu_{10}$ modes are the out-of-plane acetylenic C–H bend and asymmetric in-plane $CH_2$ bend, respectively. The larger clusters ($n > 1$) show absorptions near 3080 $cm^{-1}$ which possibly correspond to the C band of the dimer. However, this correspondence is tentative. Band A has been assigned to the overtone of $\nu_4$ which is the symmetric in-plane $CH_2$ bend. This transition shifts to the blue by about 10 $cm^{-1}$ upon $N_2$ complexation at the $CH_2$ group ($n = 2$, 3), consistent with the additional retarding force arising from the formation of the

intermolecular proton bonds. Band D at 3113 $cm^{-1}$ in the dimer spectrum is tentatively attributed to $\nu_2$ (symmetric C–H stretch of the $CH_2$ group), whereas one of the bands G or H is assigned to $\nu_3 + \nu_5$, the combination of both C–C stretch modes.

Most of the vibrational assignments given in this section are rather uncertain. Other alternative interpretations [11] may involve clusters of the less stable $C_3H_3^+$ isomers, such as $H_3CCC^+$–$(N_2)_n$ or $H_2CCHC^+$–$(N_2)_n$. In addition, as $C_3H_3^+$ has the same mass as $[CCNH]^+$ some transitions may even arise from $[CCNH]^+$–$(N_2)_n$. Although these alternative scenarios are not very likely [11], they cannot be ruled out completely on the basis of the present experimental and theoretical evidence.

### 4.4. Dissociation energies

According to the photodissociation process described in Eq. (1), several $C_3H_3^+$–$(N_2)_m$ fragment channels ($m < n$) may be observed for a given $C_3H_3^+$–$(N_2)_n$ parent cluster with $n > 1$. The number of evaporated ligands upon photoexcitation may sensitively depend on the cluster size, the excitation energy, and the type of isomer. For example, Fig. 8 shows the mass spectra obtained by mass-selecting $C_3H_3^+$–$(N_2)_3$ parent ions with the first quadrupole and scanning the mass of the second quadrupole with the laser set to different IR excitation wavelengths. For spectrum (a) the laser beam is blocked and the observed $C_3H_3^+$–$(N_2)_2$ fragment ions arise from metastable decay and/or collision-induced dissociation with residual gas in the octopole. For spectrum (b) the laser is tuned to the $\nu_1$ resonance of $H_2CCCH^+$–$(N_2)_3$ and additional laser-induced dissociation signals are observed in the $C_3H_3^+$–$(N_2)_m$ fragment channels with $m = 0$ (30%) and $m = 1$ (70%). In contrast, resonant excitation of the $\nu_4$ transition of c-$C_3H_3^+$–$(N_2)_3$ in spectrum (c) leads exclusively to the observation of $m = 0$ fragments (in addition to the $m = 2$ fragments arising from metastable decay and/or collision-induced dissociation). In general,

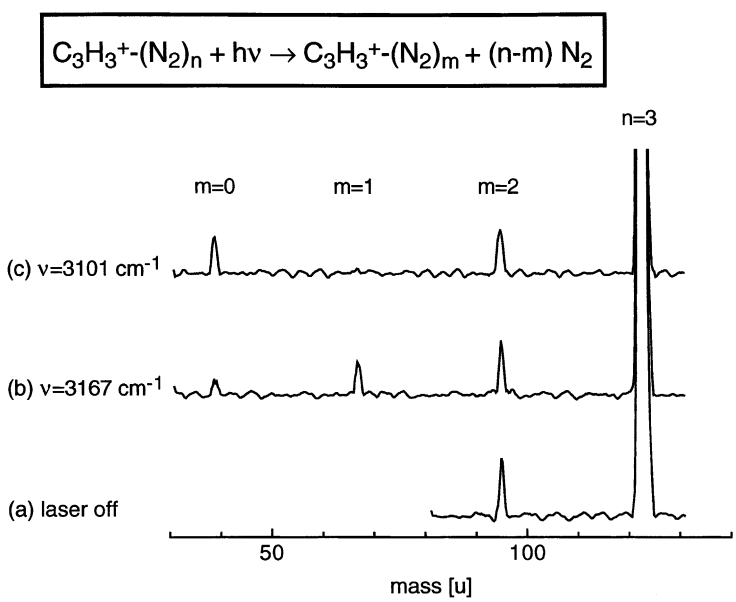


Fig. 8. Mass spectra obtained by mass selection of $C_3H_3^+$–$(N_2)_3$ with the first quadrupole mass spectrometer and scanning the mass of the second quadrupole mass spectrometer. For spectrum (a) the laser is blocked and the observed $C_3H_3^+$–$(N_2)_2$ fragment ions arise from metastable decay and/or collision-induced dissociation with residual gas in the octopole. For spectra (b) and (c) the laser is tuned to the $\nu_1$ and $\nu_4$ resonances of $H_2CCCH^+$–$(N_2)_3$ and c-$C_3H_3^+$–$(N_2)_3$, respectively, and additional laser-induced dissociation signals are observed in the $C_3H_3^+$–$(N_2)_m$ fragment channels with $m = 0$ and $m = 1$.

Table 4
Photofragmentation branching ratios (%) of $C_3H_3^+$–$(N_2)_n$ complexes for the photoinduced reaction (Eq. (1)) measured at the $\nu_4$ band of c-$C_3H_3^+$–$(N_2)_n$ and the $\nu_1$ band of $H_2CCCH^+$–$(N_2)_n$[a]

| Excitation | $n = 1, 2$ | $n = 3$ | $n = 4$ | $n = 5$ | $n = 6$ |
|---|---|---|---|---|---|
| $\nu_4$ of c-$C_3H_3^+$–$(N_2)_n$ | $m = 0$ (100) | $m = 0$ (100) | $m = 1$ (100) | $m = 2$ (100) | $m = 3$ (100) |
| $\nu_1$ of $H_2CCCH^+$–$(N_2)_n$ | $m = 0$ (100) | $m = 0$ (30), $m = 1$ (70) | $m = 1$ (100) | $m = 2$ (100) | $m = 3$ (100) |

[a] Only channels contributing more than 10% are listed. Uncertainties are estimated as 10%.

metastable decay and collision-induced dissociation leads to the evaporation of only one $N_2$ ligand, whereas laser-induced dissociation of larger $C_3H_3^+$–$(N_2)_n$ clusters ($n > 1$) causes the rupture of at least two intermolecular bonds. Typically, the fragment currents are of the order of 1% of the parent ion currents for both metastable decay/collision-activated dissociation and photoexcitation of the intense vibrational resonances at the employed laser intensities ($\approx 10^{-1}$ mJ/mm$^2$).

Table 4 summarizes the photofragmentation branching ratios measured for $\nu_1$ excitation of $H_2CCCH^+$–$(N_2)_n$ and $\nu_4$ excitation of c-$C_3H_3^+$–$(N_2)_n$. For cluster sizes with split $\nu_4$ bands ($n = 2$, 3), the ratio is measured for excitation of the more intense $\nu_4$ component. Similar to previous studies on related systems [43–50], the range of observed fragment channels is rather narrow. For nearly all cluster sizes investigated, more than 95% of the photodissociation signal appears in a single fragment channel $m$. This observation can be used for a rough estimation of ligand binding energies by assuming a simple statistical model for the evaporation process [45,48]. The basic assumption of this model is that the absorbed photon energy ($\nu_{IR} \approx 3 \times 10^3$ cm$^{-1}$) is used for ligand evaporation (only single photon absorption is observed at the employed laser intensities of $\approx 10^{-1}$ mJ/mm$^2$). Thus, the photon energy must be larger than the sum of the binding energies of the $(n - m)$ evaporated ligands but smaller than the sum of the $(n - m + 1)$ most weakly bound ligands. This model has successfully been applied to a variety of related cluster ions and has predicted dissociation energies in qualitative agreement with high level ab initio calculations and thermochemical measurements [43–50]. An additional assumption to the model is that equivalent ligands have the same binding energy. For the c-$C_3H_3^+$–$(N_2)_n$ clusters, the ligands are classified into H-bound ($n = 1$–3) and C-bound ligands ($n = 4$–9) with ligand binding energies of $D_0$(H) and $D_0$(C), respectively. The estimated binding energies derived from the photofragmentation data in Table 4 are $D_0(H) = 900 \pm 130$ cm$^{-1}$ and $D_0(C) = 860 \pm 170$ cm$^{-1}$. These values are compatible with the dissociation energies of the H-bound and C-bound c-$C_3H_3^+$–$N_2$ dimers calculated at both the B3LYP/6-31G* ($D_e = 1176$ and 793 cm$^{-1}$, Table 1) and MP2/6-311G(2df,2pd) levels ($D_e = 1227$ and 1102 cm$^{-1}$ [11]). For the $H_2CCCH^+$–$(N_2)_n$ clusters, the ligands are classified according to binding to the acetylenic CH proton ($n = 1$, $D_0$(CH)), to the $CH_2$ group ($n = 2$, 3, $D_0(CH_2)$), and further ligands ($n > 3$, $D_0(n > 3)$). The restrictions derived from the data in Table 4 are $D_0(CH) = 2000 \pm 1000$ cm$^{-1}$, $D_0(CH_2) = 1200 \pm 400$ cm$^{-1}$, and $D_0(n > 3) < 1050$ cm$^{-1}$. Again, these values are consistent with the dissociation energies of the corresponding $H_2CCCH^+$–$N_2$ dimers calculated at the B3LYP/6-31G* level, $D_e(CH) = 1381$ cm$^{-1}$ and $D_e(CH_2) = 1098$ cm$^{-1}$ (Table 2), and the MP2/6-311G(2df,2pd) level, $D_e(CH) = 1373$ cm$^{-1}$ and $D_e(CH_2) = 1180$ cm$^{-1}$ [11].

Fig. 9 compares the IR photodissociation spectra of $C_3H_3^+$–$(N_2)_3$ recorded in the $C_3H_3^+$ ($3 \rightarrow 0$) and $C_3H_3^+$–$N_2$ ($3 \rightarrow 1$) fragment channels. The intense transition assigned to the degenerate $\nu_4(e')$ fundamental of c-$C_3H_3^+$–$(N_2)_3$ (bands B/E) occurs only in the $3 \rightarrow 0$ spectrum and is completely absent in the $3 \rightarrow 1$ spectrum. In contrast, the transitions assigned to $H_2CCCH^+$–$(N_2)_3$ are observed in both spectra. Thus, the total dissociation energy of the first three

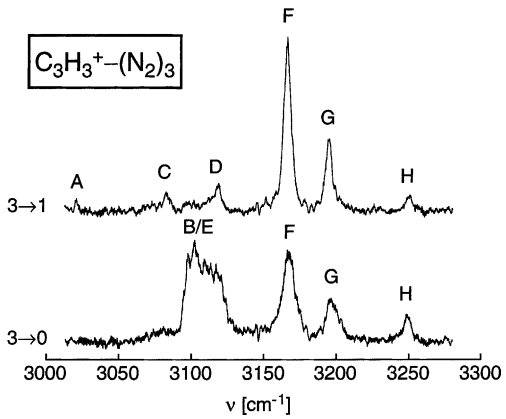


Fig. 9. IR photodissociation spectra of $C_3H_3^+$–$(N_2)_3$ recorded in the $C_3H_3^+$ (bottom) and $C_3H_3^+$–$N_2$ (top) fragment channels (indicated as $3 \rightarrow 0$ and $3 \rightarrow 1$) between 3015 and 3280 $cm^{-1}$. The observed transitions are labeled A–H and their suggested assignments are listed in Table 3. The transitions assigned to c-$C_3H_3^+$–$(N_2)_3$, B and E, occur only in the $C_3H_3^+$ fragment channel. In contrast, the (intense) transitions assigned to $H_2CCCH^+$–$(N_2)_3$ are observed in both fragment channels.

ligands in c-$C_3H_3^+$–$(N_2)_3$ must be smaller than in $H_2CCCH^+$–$(N_2)_3$. Moreover, the fact that the transitions of c-$C_3H_3^+$–$(N_2)_3$ are only observed in the $3 \rightarrow 0$ spectrum strongly suggests that all transitions seen in the $3 \rightarrow 1$ spectrum have to be attributed to another isomer. This method of isomer identification has previously also been applied to other ionic complexes [47,51]. In general, the widths of the $H_2CCCH^+$–$(N_2)_3$ transitions F, G, and H observed in the $m = 1$ fragment channel (loss of two ligands) are smaller than those in the $m = 0$ fragment channel (loss of three ligands). This effect is attributed to different internal energies of the parent cluster ions prior to IR excitation. Basically, initially colder $H_2CCCH^+$–$(N_2)_3$ cluster ions have less total internal energy after IR excitation, leading to narrower resonances and the loss of fewer ligands.

## 5. Concluding remarks

The intermolecular interaction of two important $C_3H_3^+$ isomers, namely c-$C_3H_3^+$ and $H_2CCCH^+$, with $N_2$ ligands has been characterized by IR spectroscopy of mass-selected $C_3H_3^+$–$(N_2)_n$ complexes and density functional calculations. The analysis of systematic frequency shifts and splittings as well as photofragmentation branching ratios provides a consistent picture of the microsolvation process of both hydrocarbon cations in molecular nitrogen. Detailed information about cluster geometries and structures of solvation shells is derived.

In the most stable c-$C_3H_3^+$–$(N_2)_n$ complexes, the first three $N_2$ ligands form (nearly) linear and equivalent proton bonds to the three protons of c-$C_3H_3^+$, leading to highly symmetric planar structures with $C_{2v}$ ($n = 1, 2$) and $D_{3h}$ symmetry ($n = 3$). After completion of the first subshell at $n = 3$, further $N_2$ ligands form slightly weaker intermolecular bonds to the C atoms of the almost planar c-$C_3H_3^+$–$(N_2)_3$ ion core. The dissociation energies of the H-bonds and C-bonds in c-$C_3H_3^+$–$(N_2)_n$ are estimated as $D_0(H) = 900 \pm 130\ cm^{-1}$ and $D_0(C) = 860 \pm 170\ cm^{-1}$, respectively. In general, the deduced microsolvation model of c-$C_3H_3^+$–$(N_2)_n$ is very similar to that of the related $NH_3^+$–$Ar_n$ cluster system [48,52]. In the most stable $H_2CCCH^+$–$N_2$ complex, the $N_2$ ligand forms a linear ionic H-bond to the acetylenic C–H group of $H_2CCCH^+$, leading to a planar structure with $C_{2v}$ symmetry. The calculations suggest that the next two ligands bind to the protons of the $CH_2$ group giving rise to planar structures with $C_s$ ($n = 2$) and $C_{2v}$ symmetry ($n = 3$). The binding sites of further ligands cannot be determined with the available experimental and theoretical data. For both isomeric $C_3H_3^+$–$(N_2)_n$ cluster systems, significant noncooperative three-body effects are observed, i.e., the intermolecular bonds become weaker as the cluster size increases. Moreover, large effects upon asymmetric solvation for clusters with an incomplete first solvation shell are found. Unfortunately, no matrix isolation studies of any $C_3H_3^+$ isomer in molecular nitrogen has been performed, preventing a detailed comparison of the $C_3H_3^+$–$(N_2)_n$ cluster vibrations with the bulk limit ($n \rightarrow \infty$).

Finally, the present study on $C_3H_3^+$–$(N_2)_n$ clusters demonstrates that the fruitful interplay between IR spectroscopy, mass spectrometry, and quantum chemical calculations of cluster ions can provide

fundamental information about important ions and their interaction with inert ligands. In particular, detailed knowledge of the interaction between hydrocarbon cations and $N_2$ may be useful to improve our understanding of physical and chemical phenomena in combustion processes. Moreover, concerning the unambiguous identification of isomers of ions and cluster ions, the IR spectroscopic approach employed in the present work has proven to be more generally applicable than experiments solely based on mass spectrometry.

## Acknowledgements

This study is part of project No. 20-63459.00 of the Swiss National Science Foundation. O.D. is supported by the Deutsche Forschungsgemeinschaft via a Heisenberg Fellowship (DO 729/1-1).

## References

[1] F.P. Lossing, Can. J. Chem. 50 (1972) 3973.
[2] P.J. Ausloos, S.G. Lias, J. Am. Chem. Soc. 103 (1981) 6505.
[3] M.J. McEwan, C.L. McConnell, C.G. Freeman, V.G. Anicich, J. Phys. Chem. 98 (1994) 5068.
[4] G.B.I. Scott, D.A. Fairley, C.G. Freeman, M.J. McEvan, V.G. Anicich, J. Phys. Chem. A 103 (1999) 1073.
[5] G.B.I. Scott, D.B. Milligan, D.A. Fairley, C.G. Freeman, M.J. McEvan, J. Chem. Phys. 112 (2000) 4959.
[6] R. Breslow, J.T. Groves, J. Am. Chem. Soc. 92 (1970) 984.
[7] N.C. Craig, J. Pranata, S.J. Reinganum, J.R. Sprague, P.S. Stevens, J. Am. Chem. Soc. 108 (1986) 4378.
[8] D.W. Minsek, P. Chen, J. Phys. Chem. 94 (1990) 8399.
[9] T. Gilbert, R. Pfab, I. Fischer, P. Chen, J. Chem. Phys. 112 (2000) 2575.
[10] M. Wyss, E. Riaplov, J.P. Maier, J. Chem. Phys. 114 (2001) 10355.
[11] O. Dopfer, D. Roth, J.P. Maier, J. Am. Chem. Soc. 124 (2002) 494.
[12] K. Raghavachari, R.A. Whiteside, J.A. Pople, P.V.R. Schleyer, J. Am. Chem. Soc. 103 (1981) 5649.
[13] A.C. Hopkinson, M.H. Lien, J. Am. Chem. Soc. 108 (1986) 2843.
[14] M.W. Wong, L. Radom, J. Am. Chem. Soc. 111 (1989) 6976.
[15] A. Cameron, J. Leszczynski, M.C. Zerner, B. Weiner, J. Phys. Chem. 93 (1989) 139.
[16] S.A. Maluendes, A.D. McLean, K. Yamashita, E. Herbst, J. Chem. Phys. 99 (1993) 2812.
[17] E. Herbst, N.G. Adams, D. Smith, Astrophys. J. 269 (1983) 329.
[18] N.G. Adams, D. Smith, Astrophys. J. 317 (1987) L25.
[19] D. Gerlich, S. Horning, Chem. Rev. 92 (1992) 1509.
[20] D. Smith, Chem. Rev. 92 (1992) 1473.
[21] A. Korth, M.L. Marconi, D.A. Mendis, F.R. Krueger, A.K. Richter, R.P. Lin, D.L. Mitchell, K.A. Anderson, C.W. Carlson, H. Reme, J.A. Sauvaud, C. d'Uston, Nature 337 (1989) 53.
[22] P. Thaddeus, J.M. Vritilek, C.A. Gottlieb, Astrophys. J. 299 (1985) L63.
[23] J. Cernicharo, C.A. Gottlieb, M. Guelin, T.C. Killian, G. Paubert, P. Thaddeus, J.M. Vrtilek, Astrophys. J. 368 (1991) L39.
[24] V.G. Anicich, D.B. Milligan, D.A. Fairley, M.J. McEwan, Icarus 146 (2000) 118.
[25] J.M. Goodings, D.K. Bohme, C.-W. Ng, Combust. Flame 36 (1979) 27.
[26] A.N. Hayhurst, H.R.N. Jones, Nature 296 (1982) 61.
[27] S.M. Graham, J.M. Goodings, Int. J. Mass Spectrom. Ion Process. 56 (1984) 205.
[28] V.J. Hall-Roberts, A.N. Hayhurst, D.E. Knight, S.G. Taylor, Combust. Flame 120 (2000) 578.
[29] Z. Qu, H. Zhu, Z. Li, Q. Zhang, Chem. Phys. Lett. 336 (2001) 325.
[30] P.J. Linstrom, W.G. Mallard, NIST Chemistry WebBook (National Institute of Standards and Technology, Gaithersburg, 2001, http:/webbook.nist.gov).
[31] Y. Xie, J.E. Boggs, J. Chem. Phys. 90 (1989) 4320.
[32] T.J. Lee, A. Willetts, J.F. Gaw, N.C. Handy, J. Chem. Phys. 90 (1989) 4330.
[33] S.E. Galembeck, R. Fausto, J. Mol. Struct. (Theochem.) 332 (1995) 105.
[34] P. Botschwina, M. Horn, J. Flügge, S. Seeger, J. Chem. Soc., Faraday Trans. 89 (1993) 2219.
[35] P. Botschwina, R. Oswald, J. Flügge, M. Horn, Z. Phys. Chem. 188 (1995) 29.
[36] P. Botschwina, M. Horn, R. Oswald, S. Schmatz, J. Electr. Spectrom. Rel. Phenom. 108 (2000) 109.
[37] V.G. Anicich, J. Chem. Phys. Ref. Data 22 (1993) 1469.
[38] S.A. Nizkorodov, O. Dopfer, T. Ruchti, M. Meuwly, J.P. Maier, E.J. Bieske, J. Phys. Chem. 99 (1995) 17118.
[39] G. Guelachvili, K.N. Rao, Handbook of Infrared Standards, Academic Press, London, 1993.
[40] M. J. Frisch, G. W. Trucks, H.B. Schlegel, G.E. Scuseria, M.A. Robb, J.R. Cheeseman, V.G. Zakrzewski, J.A. Montgomery, R.E. Stratman, J.C. Burant, S. Dapprich, J.M. Millam, A.D. Daniels, K.N. Kudin, M.C. Strain, O. Farkas, J. Tomasi, V. Barone, M. Cossi, R. Cammi, B. Menucci, C. Pomelli, C. Adamo, S. Clifford, J. Ochterski, G.A. Petersson, P.Y. Ayala, Q. Cui, K. Morokuma, D.K. Malick, D. Rabuck, K. Raghavachari, J.B. Foresman, J. Cioslowski, J.V. Ortiz, B.B. Stefanov, G.Liu, A. Liashenko, P. Piskorz, I. Komaromi, R. Gomperts, R.L. Martin, D.J. Fox, T. Keith, M.A. Al-Laham, C.Y. Peng, A. Nanayakkara, C. Gonzales, M. Challacombe, P.M.W. Gill, B.G. Johnson, W. Chen, M.W. Wong, J.L. Andres, C. Gonzales, M. Head-Gordon, E.S. Replogle, J.A. Pople, GAUSSIAN 98, Revision A.5, Gaussian, Inc., Pittsburgh, PA, 1998.

[41] S.F. Boys, F. Bernardi, Mol. Phys. 19 (1970) 553.
[42] S. Raugei, G. Cardini, V. Schettino, Mol. Phys. 95 (1998) 477.
[43] R.V. Olkhov, S.A. Nizkorodov, O. Dopfer, Chem. Phys. 239 (1998) 393.
[44] O. Dopfer, R.V. Olkhov, J.P. Maier, J. Phys. Chem. A 103 (1999) 2982.
[45] N. Solcà, O. Dopfer, J. Phys. Chem. A 105 (2001) 5637.
[46] R.V. Olkhov, Intermolecular Interactions in Weakly Bound Ionic Complexes Revealed by IR Photodissociation Spectroscopy, Ph.D. Thesis, University of Basel, 1999.
[47] O. Dopfer, D. Roth, J.P. Maier, J. Phys. Chem. A 104 (2000) 11702.
[48] O. Dopfer, N. Solca, R.V. Olkhov, J.P. Maier, Chem. Phys., in press.
[49] R.V. Olkhov, S.A. Nizkorodov, O. Dopfer, J. Chem. Phys. 108 (1998) 10046.
[50] O. Dopfer, S.A. Nizkorodov, M. Meuwly, E.J. Bieske, J.P. Maier, Int. J. Mass Spectrom. Ion Process. 167/168 (1997) 637.
[51] C. Chaudhuri, J.C. Jiang, X. Wang, Y.T. Lee, H.-C. Chang, J. Chem. Phys. 112 (2000) 7279.
[52] O. Dopfer, Chem. Phys., in press.